Letter

Finite-Temperature TD-DMRG for the Carrier Mobility of Organic Semiconductors

Weitang Li, Jiajun Ren, and Zhigang Shuai*

Cite This: *J. Phys. Chem. Lett.* 2020, 11, 4930−4936

Read Online

ACCESS | Metrics & More | Article Recommendations | Supporting Information

ABSTRACT: A large number of nonadiabatic dynamical studies have been applied to reveal the nature of carrier transport in organic semiconductors with different approximations. We present here a "nearly exact" graphical-process-unit-based finite-temperature time-dependent density matrix renormalization group (TD-DMRG) method to evaluate the carrier mobility in organic semiconductors, as described by the electron−phonon model, in particular, in rubrene crystal, one of the prototypical organic semiconductors, with parameters derived from first-principles. We find that (i) TD-DMRG is a general and robust method that can bridge the gap between hopping and band pictures, covering a wide range of electronic coupling strengths and (ii) with realistic parameters, TD-DMRG is able to account for the experimentally observed "band-like" transport behavior ($\partial\mu/\partial T < 0$) in rubrene. We further study the long-standing puzzle of the isotope effect for charge transport and unambiguously demonstrate that the negative isotope effect ($\partial\mu/\partial m < 0$ where m is the atomic mass) should be universal.

Nearly exact TD-DMRG

μ

Rubrene crystal

✓ Band-like transport behavior
✓ Hopping to band crossover
✓ Negative isotope effect
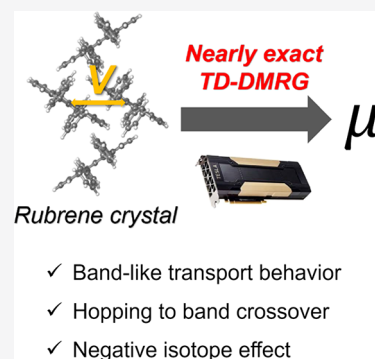
Organic semiconductors have attracted strong research interest in the scientific community due to their potential application in the next generation of electronic devices.[1] Charge mobility is a crucial physical parameter for device performance. Qualitative and quantitative descriptions of the charge-transport mechanism are essential for the molecular design of high-efficiency organic electronic devices.[2] Unfortunately, understanding the charge-transport mechanism from a microscopic point of view is of continuous debate due to the many-body electron−phonon interaction.[3−5] In the limiting cases of a strong or weak electron−phonon interaction, the charge-transport behavior can be characterized by a localized hopping picture[6,7] or a delocalized band-transport picture,[8,9] respectively, but a large class of organic semiconductors lie in the intermediate regime where the strengths of the electronic coupling and the electron−phonon interaction are comparable.[10] Although a significant amount of effort has been devoted to developing a carrier mobility theory that is applicable in the intermediate regime,[11−17] certain levels of approximation are inevitably involved, and their effect on the resulting mobility is usually unclear. For example, the approximation adopted by Hannewald and coworkers is to replace the complicated polaron-coupling operator after polaron transformation by its thermal average over the phononic part,[15] and in the transient localization theory, a relaxation time approximation is necessary to connect the carrier mobility to the correlation function of the static tight-binding model.[16,17]

In the absence of an analytical solution, a number of numerical methods have been applied to the carrier mobility problem.[5] The family of methods includes Ehrenfest dynamics,[18,19] surface hopping,[20,21] time-dependent wave packet diffusion (TDWPD),[22,23] and so on.[24−27] However, most of the methods have to sacrifice accuracy for applicability to realistic materials. For example, Ehrenfest dynamics and surface hopping treat the nuclear degree of freedom classically, and TDWPD performs truncation to the stochastic Schrödinger equation. It is only recently that numerically exact methods such as hierarchical equations of motion (HEOM)[28,29] and quantum Monte Carlo (QMC)[30] methods have been used to tackle the charge-transport problem, but these explorations are limited to model systems instead of realistic materials.

Over the past years, the density matrix renormalization group (DMRG) and its time-dependent variant (TD-DMRG) have become powerful numerically "nearly exact" solvers for quantum many-body systems.[31−34] The application of TD-DMRG to electron−phonon correlated systems has also been a great success,[35−38] achieving accuracy comparable to that of the multiconfiguration time-dependent Hartree (MCTDH) method, the de facto state-of-the-art method for nonadiabatic dynamics in complex system.[39] The latter is rarely applied for finite temperature due to the computational burden. Recently, we have implemented a highly efficient graphical-process-unit (GPU)-based finite-temperature TD-DMRG with a projector splitting algorithm for time evolution, which can tremendously

increase the computational power while keeping the "nearly exact" nature.[36,40] Now we apply this method to evaluate the carrier mobility, μ, in rubrene crystal, which is frequently studied as one of the prototypical organic semiconductor materials.[41] Our calculation based on first-principle parameters predicts "band-like" transport behavior $\left(\frac{\partial \mu}{\partial T} < 0\right)$ for the rubrene crystal, which is in agreement with experimental observations.[42−44] Additionally, we find that if the electronic coupling is set to be an adjustable parameter, then TD-DMRG is able to bridge the gap between hopping and band pictures by reproducing the analytical formula in the hopping limit and approaching the asymptotic behavior in the band limit. We further apply the method to study the long-standing puzzle of isotope effect for charge transport pioneered by Munn et al. in 1970[45] and confirm the negative isotope effect[46] $(\partial \mu / \partial m < 0$ where m is the atomic mass) caused by the reduced polaron size.

Theoretical investigations have revealed that in the rubrene crystal, the electronic coupling and the hole mobility (predicted by the TDWPD method) in the stacking direction are much larger than those in other directions,[47−49] so we map the rubrene crystal to a 1D multimode Holstein model. The 1D approximation is commonly adopted by researchers when new methodologies to compute mobility are proposed.[20,47,50] The Hamiltonian of the model reads

$$\hat{H} = \hat{H}_e + \hat{H}_{ph} + \hat{H}_{e-ph}$$

$$\hat{H}_e = V \sum_n (c_{n+1}^\dagger c_n + c_n^\dagger c_{n+1})$$

$$\hat{H}_{ph} = \sum_{n,m} \omega_m b_{n,m}^\dagger b_{n,m}$$

$$\hat{H}_{e-ph} = \sum_{n,m} g_m \omega_m (b_{n,m}^\dagger + b_{n,m}) c_n^\dagger c_n \quad (1)$$

where $c^\dagger$ (c) and $b^\dagger$ (b) are the creation (annihilation) operators for the electron and the phonon, respectively, V is the electronic coupling (also known as the transfer integral), ω_m is the frequency of the mth normal mode, and g_m is the dimensionless electron−phonon coupling constant between the mth mode and the electronic degree of freedom. In this Letter, we use $V = 83$ meV and nine vibration modes for each molecule with vibration frequency ranging from 84 to 1594 cm^{-1} and the total reorganization energy $\lambda = \sum_m \lambda_m = \sum_m g_m^2 \omega_m$ = 75 meV unless otherwise stated. The parameters are adopted from our previous work.[48] The ω_m and λ_m for each vibration modes are shown in the Supporting Information. It should be noted that in a number of publications, off-diagonal electron− phonon coupling (also known as Peierls coupling or dynamic disorder) is considered to be dominant in rubrene crystal;[17,47] however, the conclusion is drawn from quite approximate methodologies such as Ehrenfest dynamics and should be subjected to verification by higher level methods. At the end of this Letter, we demonstrate that TD-DMRG can be generalized to models with off-diagonal electron−phonon coupling, and we leave a thorough investigation of the controversial role of off-diagonal electron−phonon coupling in organic semiconductors[20,26,28,51] to future work.

The carrier mobility is obtained via the Kubo formula[4]

$$\mu = \frac{1}{2k_B T e_0} \int_{-\infty}^{\infty} \langle \hat{j}(t)\hat{j}(0)\rangle \, dt = \frac{1}{2k_B T e_0} \int_{-\infty}^{\infty} C(t) \, dt \quad (2)$$

where for the Holstein Hamiltonian

$$\hat{j} = \frac{e_0 V R}{i} \sum_n (c_{n+1}^\dagger c_n - c_n^\dagger c_{n+1}) \quad (3)$$

Here R is the intermolecular distance. With the nine-mode Holstein Hamiltonian for the rubrene crystal, $C(t)$ rapidly decays to nearly zero before 6000 au, as shown in Figure 1. We
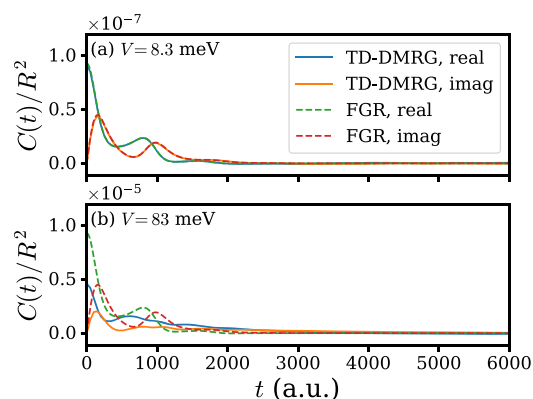

Figure 1. Comparison of the correlation function $C(t)/R^2$ obtained by TD-DMRG (solid lines) and the analytical formula eq 7 derived from FGR valid at the hopping limit (dashed lines). (a) V is set to 8.3 meV, where an analytical solution is available to demonstrate the accuracy of the TD-DMRG method. (b) V is set to 83 meV, which is the actual parameter for the rubrene crystal. $C(t)/R^2$ is in atomic units.

note that $C(t)$ is expected to show some kind of Poincaré recurrence because we have treated the rubrene crystal as a closed system. However, the recurrence is unlikely to happen for realistic materials due to the presence of various dissipations. Therefore, when integrating the correlation function, the integration time limit is set to the nearly zero region before the recurrence time to exclude the effect of the artificial recurrence. An example of the recurrence is included in the Supporting Information.

The evaluation of the current−current correlation function $C(t) = \langle \hat{j}(t)\hat{j}(0)\rangle$ is performed by TD-DMRG through imaginary and real-time propagation. The basic idea behind TD-DMRG in the language of the matrix product state (MPS) and matrix product operator (MPO) has already been reviewed in detail,[33,34] and a short overview can be found in the Supporting Information. Here we only briefly summarize the finite-temperature algorithm based on thermal field dynamics, also known as the purification method.[33,52] The thermal equilibrium density matrix of any mixed state in physical space P can be expressed as a partial trace over an enlarged Hilbert space $P \otimes Q$, where Q is an auxiliary space chosen to be a copy of P. The thermal equilibrium density operator is then expressed as a partial trace of the pure state Ψ_β in the enlarged Hilbert space over the Q space

$$\hat{\rho}_\beta = \frac{e^{-\beta \hat{H}}}{Z} = \frac{Tr_Q |\Psi_\beta\rangle\langle\Psi_\beta|}{Tr_{PQ}|\Psi_\beta\rangle\langle\Psi_\beta|} \quad (4)$$

and the pure state $|\Psi_\beta\rangle$ represented as an MPS is obtained by the imaginary time propagation from the locally maximally entangled state $|I\rangle = \sum_i |i\rangle_P |i\rangle_Q$ to $\beta/2$

$$|\Psi_\beta\rangle = e^{-\beta\hat{H}/2}|I\rangle \tag{5}$$

To calculate $C(t)$, $|\Psi_\beta\rangle$ and $\hat{j}(0)|\Psi_\beta\rangle$ are propagated in real time to obtain $e^{-i\hat{H}t}|\Psi_\beta\rangle$ and $e^{-i\hat{H}t}\hat{j}(0)|\Psi_\beta\rangle$, and then $C(t)$ is calculated by

$$C(t) = \langle\Psi_\beta|e^{i\hat{H}t}\hat{j}(0)e^{-i\hat{H}t}\hat{j}(0)|\Psi_\beta\rangle/Z \tag{6}$$

Here the current operator $\hat{j}(0)$ is represented as an MPO, and the inner product for $|\Psi_\beta\rangle$ includes tracing over both the P space and the Q space. In principle, both imaginary and real-time propagation can be carried out by any time evolution methods available to TD-DMRG.[34] In this work, we use the time-dependent variational-principle-based projector splitting time evolution scheme,[53] which is found to be relatively efficient and accurate in our recent work.[40] Readers are also referred to our previous work on finite-temperature TD-DMRG[36] for more computational details. In most of our simulations, the number of molecules in the periodic 1D chain is 21, and the bond dimension is 32. In certain cases, we find a larger system size and bond dimension necessary, such as at low temperature ($T = 200$ K) or large electronic coupling ($V = 500$ meV).

Before presenting the calculated mobility for the rubrene crystal, we show in Figure 1a the benchmark for the TD-DMRG method by comparing the correlation function calculated at $V = 8.3$ meV with an analytical solution valid in the hopping limit obtained from Fermi's Golden Rule (FGR)[7]

$$C(t)/R^2 = V^2 \exp\left\{-\sum_m g_m^2[2n_m + 1 - n_m e^{-i\omega_m t} - (n_m + 1)e^{i\omega_m t}]\right\} \tag{7}$$

where n_m is the thermal average occupation number of the mth vibrational mode at a given temperature. We can see from Figure 1a that in the hopping limit, TD-DMRG is able to reproduce the analytical formula with impressive precision. The two curves by TD-DMRG and eq 7 exactly coincide with each other for both the real and imaginary parts. We also show in Figure 1b the same comparison but with $V = 83$ meV, the actual parameter of the rubrene crystal that is in the intermediate regime. For parameters of realistic material, eq 7 clearly fails, and a more accurate method is required.

Figure 2 shows the carrier mobility of rubrene crystal obtained from TD-DMRG at various temperatures along with results from the experiment.[44] The "band-like" transport behavior in which the mobility decreases with temperature is captured by TD-DMRG, and the absolute mobility value (47 cm²/V·s) at $T = 300$ K closely matches the highest experimental report (40 cm²/V·s).[54] Nevertheless, the most commonly reported experimental room-temperature mobility for rubrene crystal is around 15−20 cm²/V·s.[44,55−57] It should be noted that for a number of organic semiconductors including pentacene, the measured mobility has been increased by a factor of ∼40 in the past two decades.[58,59] A direct comparison with experimental values should also include both static and possibly dynamic off-diagonal disorders. For comparison with TD-DMRG results, two widely used methods valid, respectively, at the incoherent hopping regime and the coherent band regime are also shown in Figure 2. In the
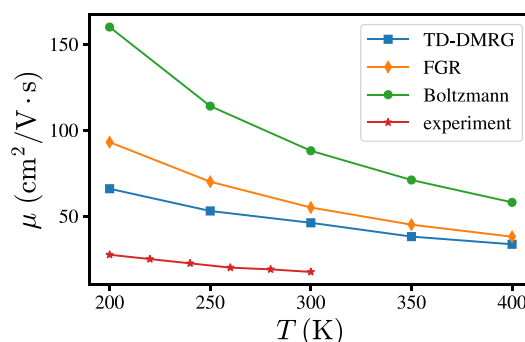

Figure 2. Carrier mobility of rubrene crystal from $T = 200$ to 400 K obtained from TD-DMRG along with experimental results.[44] The results obtained from FGR and the Boltzmann transport theory are also shown for comparison, which are, respectively, valid at the hopping regime and the band regime.

hopping regime, the carrier diffusion is described as site-to-site hopping with transition rates given by FGR,[7] whereas the carrier mobility in the band regime is described by the Boltzmann transport theory with relaxation time determined by the first-order perturbation treatment of the electron−phonon interaction. Although it is natural for the Boltzmann transport theory to predict "band-like" behavior, the same is not true for the hopping model unless the nuclear tunnelling effect is taken into account, which becomes weaker at higher temperature, and thus the mobility decreases with temperature.[7] Figure 2 also shows that although both FGR and the Boltzmann transport theory overestimate the carrier mobility, the prediction by FGR is more accurate than the Boltzmann transport theory, especially at high temperature. The observation naturally leads to the question, at which strength of electronic coupling does the delocalized band picture better describe the transport mechanism than the localized hopping picture? Therefore, in Figure 3a, we further compare TD-DMRG, FGR, and the Boltzmann transport theory from weak to strong electronic coupling while holding the electron−phonon coupling strength constant. When $V \ll \lambda$, we find that TD-DMRG reproduces FGR results perfectly, as expected from the benchmark result in Figure 1a. As the electronic
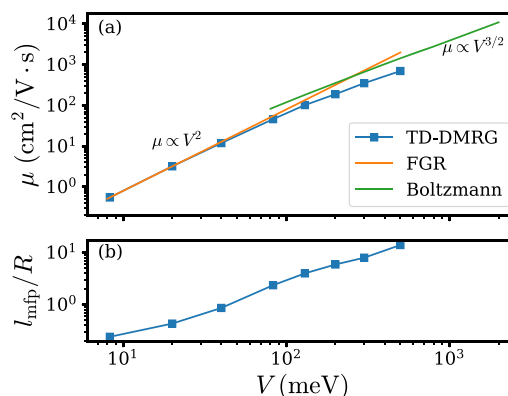

Figure 3. (a) Carrier mobility from weak to strong electronic coupling (V) calculated by TD-DMRG, FGR (hopping limit), and Boltzmann transport theory (band limit). (b) Mean free path (l_{mfp}) of the charge carrier from weak to strong electronic coupling calculated by TD-DMRG. In both panels the electron−phonon coupling parameters are adopted from the first-principle calculation of rubrene crystal.

coupling increases, the carrier mobility predicted by FGR increases quadratically, whereas the TD-DMRG result increases subquadratically, leading to a noticeable difference between the two methods at $V = 83$ meV, the actual electronic coupling in rubrene crystal. At this point, the delocalized band picture sets in and shows a $\mu \propto V^{3/2}$ behavior.[8] Accordingly, the slope of the TD-DMRG curve gradually changes from 2 to $\frac{3}{2}$, and the carrier mobility by TD-DMRG further deviates from the FGR result. Unfortunately we cannot reproduce the band limit as accurately as the hopping limit because of the computationally prohibitive bond dimension required for large V, and we estimate that the data for $V = 500$ meV has an error larger than 10%. In this regime, FGR predicts a spurious $\mu \propto V^2$ growth and finally yields mobility higher than the band description at $V > 200$ meV, indicating the complete failure of the perturbation treatment of the electronic coupling. However, with $V \approx 100$ meV, FGR still gives a quite reasonable value of the carrier mobility, although the electronic coupling is already too large to be formally considered as a perturbation.[10] We speculate that the success of the hopping picture might be partly ascribed to the cancellation of errors; that is, the fast quadratic growth compensates for the drawback of neglecting the contribution from the coherent transport. In Figure 3b, we have shown the mean free path ($l_{mfp} = v\tau$) of the charge carrier calculated by TD-DMRG with the group velocity, v, and relaxation time, τ, estimated by[27]

$$v = \sqrt{\langle \hat{j}(0)\hat{j}(0) \rangle}$$

$$\tau = \frac{1}{2}\int_{-\infty}^{\infty} \left| \frac{\text{Re}C(t)}{\text{Re}C(0)} \right| dt \qquad (8)$$

We find that when $V < 20$ meV, l_{mfp}/R is smaller than 1, so a localized hopping picture is well-suited for this regime. For the actual parameter of the rubrene crystal ($V = 83$ meV), l_{mfp}/R is found to be 2.4, which indicates that neither the hopping nor the band picture is perfectly suitable for this regime, and an unbiased method like TD-DMRG is necessary.

The isotope effect for charge transport is controversial in that a number of methods predict different results. Here we use the numerically exact TD-DMRG method to study the isotope effect for charge transport in the rubrene crystal. Our previous work points out that the nuclear tunneling effect plays an indispensable role in the isotope effect.[46] In this regard, TD-DMRG serves as a suitable tool because it treats both the electronic and vibrational degrees of freedom on an equal footing quantum mechanically. In this work, we use two different approaches to simulate isotope substitution, and they eventually lead to the same conclusion. The first approach is to perform a first-principles quantum chemistry calculation on an isotope-substituted rubrene molecule to obtain new sets of parameters for eq 1, as shown in Figure 4a. To preclude the effect of numerical error, we also calculated the mobility of a hypothetical rubrene where the atomic mass of carbon is 20 amu. The second approach to simulate the isotope effect is to scale all vibration frequencies in native rubrene by a constant factor while holding the respective reorganization energy constant, as illustrated in Figure 4b. The calculated mobility by the two approaches shows that TD-DMRG predicts a negative isotope effect, which is in agreement with the experimental result.[44] The absolute value of the isotope effect
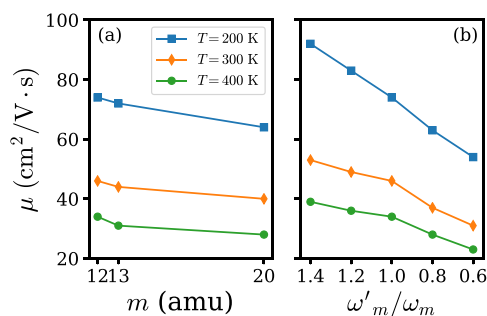

Figure 4. Isotope effect on charge transport in the rubrene crystal from $T = 200$ to 400 K. (a) Carrier mobility with increasing carbon mass, m, and the respective ω_m and λ_m are obtained by first-principle calculations. (b) Carrier mobility at different vibrational frequencies ω'_m, with the original frequencies ω_m as the unit and λ_m held as a constant.

$\left(\frac{\mu'}{\mu} - 1\right) \times 100\%$ for ^{13}C substitution is found to be $\sim$4% by TD-DMRG.

To further analyze the origin of the negative isotope effect from the TD-DMRG point of view, we calculated the coherent length, L, from the reduced thermal equilibrium density operator $\sigma = \text{Tr}_{ph}\{\rho_\beta\}$ defined as[60]

$$L = \frac{\left(\sum_{ij}^{N} |\sigma_{ij}|\right)^2}{N\sum_{ij}^{N} |\sigma_{ij}|^2} \qquad (9)$$

For a completely localized thermal equilibrium state, no coherence is present, so $|\sigma_{ij}| = N^{-1}\delta_{ij}$ and $L = 1$. For a completely delocalized thermal equilibrium state, $|\sigma_{ij}| = N^{-1}$ and $L = N$. So L measures the length scale of the charge delocalization or the polaron size. The calculated L for different vibrational frequencies representing the effect of isotopic substitution is shown in Figure 5. For temperature ranging from $T = 250$ to 350 K, L decreases as ω_m'/ω_m decreases, which implies that heavy isotopic substitution reduces the polaron size.
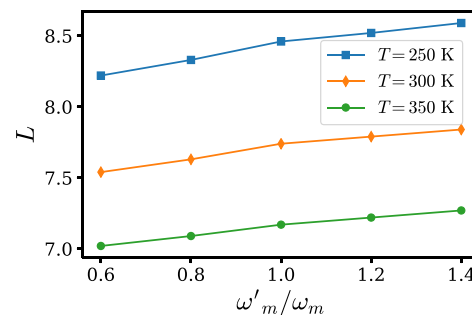

Figure 5. Coherent length, L, defined in eq 9 at different vibrational frequencies from 250 to 350 K. λ_m for each mode is held as a constant.

Finally, we move on to discuss off-diagonal disorder, as it has been proposed as the dominant mechanism for transport, which was not included in the model Hamiltonian eq 1. This is an interesting mechanism, already proposed by Munn and Silbey in 1980[61,62] and strongly revived recently.[17,18] Our previous study based on molecular dynamics and the quantum-tunneling-enabled hopping model for pentacene indicated that dynamic disorder can indeed limit transport in the 1D model

but not for higher dimensions, a conclusion in accordance with Anderson's theorem.[51] Thus a comprehensive consideration of the off-dynamic disorder should be carried out in high dimensions. So far, our TD-DMRG algorithm is structured for the 1D case. For the 2D case, a tensor-network-type renormalization scheme could be considered, but the computational complexity is much higher, and it deserves further efforts to develop efficient algorithms. But in a preliminary attempt to unravel the off-diagonal term in the present study of the 1D case, we set $V = 8.3$ meV in the hopping limit so that we can compare with our previous case study.[51] The off-diagonal electron−phonon coupling is included in the system via the Holstein−Peierls Hamiltonian, similar to eq 1, except that $\hat{H}_{e-ph}$ becomes

$$\hat{H}_{e-ph} = \sum_{n,m} g_m^{(1)} \omega_m (b_{n,m}^\dagger + b_{n,m}) c_n^\dagger c_n$$
$$+ \sum_{n,m} g_m^{(2)} \omega_m (b_{n,m}^\dagger + b_{n,m})(c_n^\dagger c_{n+1} + c_{n+1}^\dagger c_n)$$

(10)

Here we assume that $g_m^{(1)} g_m^{(2)} = 0$ and only one mode contributes to the Peierls coupling. The parameters of intramolecular vibration are adopted from the four-mode parameters shown in the Supporting Information, and the frequency of the intermolecular vibration mode is set to 50 cm^{-1}. The mobility calculated by TD-DMRG as a function of the standard deviation of the transfer integral (ΔV) over the mean transfer integral (V) is shown in Figure 6. We consider
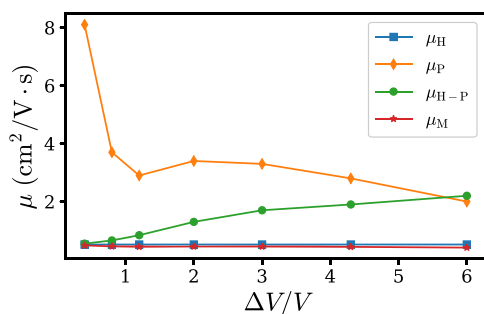

Figure 6. Carrier mobility as a function of the standard deviation of the transfer integral (ΔV) over the mean transfer integral (V). μ_H denotes the mobility with only Holstein coupling, μ_P denotes the mobility with only Peierls coupling, μ_{H-P} denotes the mobility with both Holstein and Peierls coupling, and μ_M is obtained by Matthiessen's rule, $1/\mu_M = 1/\mu_H + 1/\mu_P$.

mobilities with three kinds of electron−phonon coupling paradigms in Figure 6: (1) mobility with only Holstein coupling, μ_H, (2) mobility with only Peierls coupling, μ_P, and (3) mobility with both Holstein and Peierls coupling, μ_{H-P}. With only Holstein coupling, there is actually no transfer integral fluctuation, and μ_H is a constant. With only Peierls coupling, μ_P first decreases, then increases, and finally decreases again. In the absence of Holstein coupling, μ_P in the $\Delta V \to 0$ limit approaches infinity, which is why μ_P first decreases. The subsequent increase and decrease can be ascribed to the stronger phonon-assisted current at the larger ΔV and the disorder limited charge transport when $\Delta V \to \infty$, respectively. On the contrary, μ_{H-P} steadily grows from $\Delta V/V = 0.4$ to 8 due to the phonon-assisted current. We also show in Figure 6 the mobility obtained by Matthiessen's rule $1/\mu_M = 1/\mu_H + 1/\mu_P$, and we find out that although the rule is

applicable at a small ΔV limit, it fails to describe the phonon-assisted current, which is dominant at a large ΔV regime. Our result is consistent with our previous report.[51]

In summary, we have demonstrated that the finite-temperature TD-DMRG works as a general and powerful tool to calculate the carrier mobility for organic semiconductors covering a wide range of electron−phonon coupling strengths from the hopping to the band regimes. When coupled to molecular parameters from the first-principles calculation, taking rubrene as an example, TD-DMRG successfully accounts for the experimentally observed "band-like" transport behavior. The long-standing controversy over the isotope effect on mobility was definitely demonstrated to be negative. We also carefully carried out a comparison with the well-established solutions at the hopping and band limits and found that TD-DMRG is able to reproduce the analytical result in the hopping limit and approach the asymptotic behavior in the band limit. Lastly, we show that TD-DMRG is able to take off-diagonal electron−phonon coupling into consideration, as TD-DMRG is quite a general approach. However, a comprehensive description of the off-diagonal disorder should go to a higher dimension for more general molecular parameters, an intriguing subject for future work.

■ ASSOCIATED CONTENT

ⓢ Supporting Information

The Supporting Information is available free of charge at https://pubs.acs.org/doi/10.1021/acs.jpclett.0c01072.

Vibrational modes of the rubrene molecule, Poincaré recurrence observed in the hopping limit, and a brief overview of TD-DMRG algorithm (PDF)

■ AUTHOR INFORMATION

Corresponding Author

Zhigang Shuai − MOE Key Laboratory of Organic OptoElectronics and Molecular Engineering, Department of Chemistry, Tsinghua University, Beijing 100084, People's Republic of China; ⓞ orcid.org/0000-0003-3867-2331; Email: zgshuai@tsinghua.edu.cn

Authors

Weitang Li − MOE Key Laboratory of Organic OptoElectronics and Molecular Engineering, Department of Chemistry, Tsinghua University, Beijing 100084, People's Republic of China; ⓞ orcid.org/0000-0002-8739-641X

Jiajun Ren − MOE Key Laboratory of Organic OptoElectronics and Molecular Engineering, Department of Chemistry, Tsinghua University, Beijing 100084, People's Republic of China; ⓞ orcid.org/0000-0002-1508-4943

Complete contact information is available at:
https://pubs.acs.org/10.1021/acs.jpclett.0c01072

Notes

The authors declare no competing financial interest.

■ ACKNOWLEDGMENTS

■ REFERENCES

(1) Forrest, S. R. The Path to Ubiquitous and Low-Cost Organic Electronic Appliances on Plastic. *Nature* **2004**, *428*, 911−918.

(2) Coropceanu, V.; Cornil, J.; da Silva Filho, D. A.; Olivier, Y.; Silbey, R.; Brédas, J.-L. Charge Transport in Organic Semiconductors. *Chem. Rev.* **2007**, *107* (4), 926−952.

(3) Kenkre, V. M.; Reineker, P. *Exciton Dynamics in Molecular Crystals and Aggregates*; Springer: Berlin, 1982.

(4) Mahan, G. D. *Many-Particle Physics*; Springer: Boston, 2000.

(5) Oberhofer, H.; Reuter, K.; Blumberger, J. Charge Transport in Molecular Materials: An Assessment of Computational Methods. *Chem. Rev.* **2017**, *117*, 10319−10357.

(6) Holstein, T. Studies of Polaron Motion: Part II. The "Small" Polaron. *Ann. Phys.* **1959**, *8*, 343−389.

(7) Nan, G.; Yang, X.; Wang, L.; Shuai, Z.; Zhao, Y. Nuclear Tunneling Effects of Charge Transport in Rubrene, Tetracene, and Pentacene. *Phys. Rev. B: Condens. Matter Mater. Phys.* **2009**, *79*, 115203.

(8) Glarum, S. H. Electron Mobilities in Organic Semiconductors. *J. Phys. Chem. Solids* **1963**, *24*, 1577−1583.

(9) Xi, J.; Long, M.; Tang, L.; Wang, D.; Shuai, Z. First-Principles Prediction of Charge Mobility in Carbon and Organic Nanomaterials. *Nanoscale* **2012**, *4*, 4348−4369.

(10) Troisi, A. Charge Transport in High Mobility Molecular Semiconductors: Classical Models and New Theories. *Chem. Soc. Rev.* **2011**, *40*, 2347−2358.

(11) Silbey, R.; Munn, R. General Theory of Electronic Transport in Molecular Crystals. I. Local Linear Electron−Phonon Coupling. *J. Chem. Phys.* **1980**, *72*, 2763−2773.

(12) Kenkre, V.; Andersen, J. D.; Dunlap, D.; Duke, C. Unified Theory of the Mobilities of Photoinjected Electrons in Naphthalene. *Phys. Rev. Lett.* **1989**, *62*, 1165.

(13) Giuggioli, L.; Andersen, J. D.; Kenkre, V. M. Mobility Theory of Intermediate-Bandwidth Carriers in Organic Crystals: Scattering by Acoustic and Optical Phonons. *Phys. Rev. B: Condens. Matter Mater. Phys.* **2003**, *67*, 045110.

(14) Hannewald, K.; Stojanović, V.; Schellekens, J.; Bobbert, P.; Kresse, G.; Hafner, J. Theory of Polaron Bandwidth Narrowing in Organic Molecular Crystals. *Phys. Rev. B: Condens. Matter Mater. Phys.* **2004**, *69*, 075211.

(15) Ortmann, F.; Bechstedt, F.; Hannewald, K. Theory of Charge Transport in Organic Crystals: Beyond Holstein's Small-Polaron Model. *Phys. Rev. B: Condens. Matter Mater. Phys.* **2009**, *79*, 235206.

(16) Fratini, S.; Mayou, D.; Ciuchi, S. The Transient Localization Scenario for Charge Transport in Crystalline Organic Materials. *Adv. Funct. Mater.* **2016**, *26*, 2292−2315.

(17) Fratini, S.; Ciuchi, S.; Mayou, D.; de Laissardière, G. T.; Troisi, A. A Map of High-mobility Molecular Semiconductors. *Nat. Mater.* **2017**, *16*, 998−1002.

(18) Troisi, A.; Orlandi, G. Charge-Transport Regime of Crystalline Organic Semiconductors: Diffusion Limited by Thermal Off-Diagonal Electronic Disorder. *Phys. Rev. Lett.* **2006**, *96*, 086601.

(19) Ciuchi, S.; Fratini, S.; Mayou, D. Transient Localization in Crystalline Organic Semiconductors. *Phys. Rev. B: Condens. Matter Mater. Phys.* **2011**, *83*, 081202.

(20) Wang, L.; Beljonne, D. Flexible Surface Hopping Approach to Model the Crossover From Hopping to Band-Like Transport in Organic Crystals. *J. Phys. Chem. Lett.* **2013**, *4*, 1888−1894.

(21) Giannini, S.; Carof, A.; Ellis, M.; Yang, H.; Ziogos, O. G.; Ghosh, S.; Blumberger, J. Quantum Localization and Delocalization of Charge Carriers in Organic Semiconducting Crystals. *Nat. Commun.* **2019**, *10*, 3843.

(22) Zhong, X.; Zhao, Y. Non-Markovian Stochastic Schrödinger Equation at Finite Temperatures for Charge Carrier Dynamics in Organic Crystals. *J. Chem. Phys.* **2013**, *138*, 014111.

(23) Zhong, X.; Zhao, Y.; Cao, J. Coherent Quantum Transport in Disordered Systems: II. Temperature Dependence of Carrier Diffusion Coefficients From the Time-Dependent Wavepacket Diffusion Method. *New J. Phys.* **2014**, *16*, 045009.

(24) Fratini, S.; Ciuchi, S. Bandlike Motion and Mobility Saturation in Organic Molecular Semiconductors. *Phys. Rev. Lett.* **2009**, *103*, 266601.

(25) Moix, J. M.; Khasin, M.; Cao, J. Coherent Quantum Transport in Disordered Systems: I. The Influence of Dephasing on the Transport Properties and Absorption Spectra on One-Dimensional Systems. *New J. Phys.* **2013**, *15*, 085010.

(26) Song, L.; Shi, Q. A New Approach to Calculate Charge Carrier Transport Mobility in Organic Molecular Crystals From Imaginary Time Path Integral Simulations. *J. Chem. Phys.* **2015**, *142*, 174103.

(27) Prodanović, N.; Vukmirović, N. Charge Carrier Mobility in Systems with Local Electron-Phonon Interaction. *Phys. Rev. B: Condens. Matter Mater. Phys.* **2019**, *99*, 104304.

(28) Wang, D.; Chen, L.; Zheng, R.; Wang, L.; Shi, Q. Communications: A Nonperturbative Quantum Master Equation Approach to Charge Carrier Transport in Organic Molecular Crystals. *J. Chem. Phys.* **2010**, *132*, 081101.

(29) Yan, Y.; Xu, M.; Liu, Y.; Shi, Q. Theoretical Study of Charge Carrier Transport in Organic Molecular Crystals Using the Nakajima-Zwanzig-Mori Generalized Master Equation. *J. Chem. Phys.* **2019**, *150*, 234101.

(30) Mishchenko, A. S.; Nagaosa, N.; De Filippis, G.; de Candia, A.; Cataudella, V. Mobility of Holstein Polaron at Finite Temperature: An Unbiased Approach. *Phys. Rev. Lett.* **2015**, *114*, 146401.

(31) White, S. R. Density Matrix Formulation for Quantum Renormalzation Groups. *Phys. Rev. Lett.* **1992**, *69*, 2863.

(32) Jeckelmann, E.; White, S. R. Density-Matrix Renormalization-Group Study of the Polaron Problem in the Holstein Model. *Phys. Rev. B: Condens. Matter Mater. Phys.* **1998**, *57*, 6376.

(33) Schollwöck, U. The Density-Matrix Renormalization Group in the Age of Matrix Product States. *Ann. Phys.* **2011**, *326*, 96−192.

(34) Paeckel, S.; Köhler, T.; Swoboda, A.; Manmana, S. R.; Schollwöck, U.; Hubig, C. Time-Evolution Methods for Matrix-Product States. *Ann. Phys.* **2019**, *411*, 167998.

(35) Prior, J.; Chin, A. W.; Huelga, S. F.; Plenio, M. B. Efficient Simulation of Strong System-Environment Interactions. *Phys. Rev. Lett.* **2010**, *105*, 050404.

(36) Ren, J.; Shuai, Z.; Kin-Lic Chan, G Time-Dependent Density Matrix Renormalization Group Algorithms for Nearly Exact Absorption and Fluorescence Spectra of Molecular Aggregates at Both Zero and Finite Temperature. *J. Chem. Theory Comput.* **2018**, *14*, 5027−5039.

(37) Xie, X.; Liu, Y.; Yao, Y.; Schollwöck, U.; Liu, C.; Ma, H. Time-Dependent Density Matrix Renormalization Group Quantum Dynamics for Realistic Chemical Systems. *J. Chem. Phys.* **2019**, *151*, 224101.

(38) Baiardi, A.; Reiher, M. Large-Scale Quantum Dynamics with Matrix Product States. *J. Chem. Theory Comput.* **2019**, *15*, 3481−3498.

(39) Beck, M. H.; Jäckle, A.; Worth, G. A.; Meyer, H.-D. The Multiconfiguration Time-Dependent Hartree (MCTDH) Method: A Highly Efficient Algorithm for Propagating Wavepackets. *Phys. Rep.* **2000**, *324*, 1−105.

(40) Li, W.; Ren, J.; Shuai, Z. Numerical Assessment for Accuracy and GPU Acceleration of TD-DMRG Time Evolution Schemes. *J. Chem. Phys.* **2020**, *152*, 024127.

(41) Ordejón, P.; Boskovic, D.; Panhans, M.; Ortmann, F. Ab Initio Study of Electron-Phonon Coupling in Rubrene. *Phys. Rev. B: Condens. Matter Mater. Phys.* **2017**, *96*, 035202.

(42) Podzorov, V.; Menard, E.; Rogers, J. A.; Gershenson, M. E. Hall Effect in the Accumulation Layers on the Surface of Organic Semiconductors. *Phys. Rev. Lett.* **2005**, *95*, 226601.

(43) Machida, S.-i.; Nakayama, Y.; Duhm, S.; Xin, Q.; Funakoshi, A.; Ogawa, N.; Kera, S.; Ueno, N.; Ishii, H. Highest-Occupied-Molecular-Orbital Band Dispersion of Rubrene Single Crystals as Observed by

Angle-Resolved Ultraviolet Photoelectron Spectroscopy. *Phys. Rev. Lett.* **2010**, *104*, 156401.

(44) Ren, X.; Bruzek, M. J.; Hanifi, D. A.; Schulzetenberg, A.; Wu, Y.; Kim, C.-H.; Zhang, Z.; Johns, J. E.; Salleo, A.; Fratini, S.; et al. Negative Isotope Effect on Field-Effect Hole Transport in Fully Substituted ^{13}C-Rubrene. *Adv. Electron. Mater.* **2017**, *3*, 1700018.

(45) Munn, R. W.; Siebrand, W. Transport of Quasilocalized Exicitons in Molecular Crystals. *J. Chem. Phys.* **1970**, *52*, 47−63.

(46) Jiang, Y.; Shuai, Z.; Liu, M. The Isotope Effect on Charge Transport for Bithiophene and Di(n-Hexyl)-Bithiophene: Impacts of Deuteration Position, Deuteration Number and Side Chain Substitution Position. *Theor. Chem. Acc.* **2018**, *137*, 33.

(47) Troisi, A. Prediction of the Absolute Charge Mobility of Molecular Semiconductors: The Case of Rubrene. *Adv. Mater.* **2007**, *19*, 2000−2004.

(48) Jiang, Y.; Zhong, X.; Shi, W.; Peng, Q.; Geng, H.; Zhao, Y.; Shuai, Z. Nuclear Quantum Tunnelling and Carrier Delocalization Effects to Bridge the Gap Between Hopping and Bandlike Behaviors in Organic Semiconductors. *Nanoscale Horiz* **2016**, *1*, 53−59.

(49) Xie, X.; Santana-Bonilla, A.; Troisi, A. Nonlocal Electron−Phonon Coupling in Prototypical Molecular Semiconductors From First Principles. *J. Chem. Theory Comput.* **2018**, *14*, 3752−3762.

(50) Ciuchi, S.; Fratini, S. Electronic Transport and Quantum Localization Effects in Organic Semiconductors. *Phys. Rev. B: Condens. Matter Mater. Phys.* **2012**, *86*, 245201.

(51) Wang, L.; Li, Q.; Shuai, Z.; Chen, L.; Shi, Q. Multiscale Study of Charge Mobility of Organic Semiconductor with Dynamic Disorders. *Phys. Chem. Chem. Phys.* **2010**, *12*, 3309−3314.

(52) Feiguin, A. E.; White, S. R. Finite-Temperature Density Matrix Renormalization Using an Enlarged Hilbert Space. *Phys. Rev. B: Condens. Matter Mater. Phys.* **2005**, *72*, 220401.

(53) Haegeman, J.; Lubich, C.; Oseledets, I.; Vandereycken, B.; Verstraete, F. Unifying Time Evolution and Optimization with Matrix Product States. *Phys. Rev. B: Condens. Matter Mater. Phys.* **2016**, *94*, 165116.

(54) Takeya, J.; Yamagishi, M.; Tominari, Y.; Hirahara, R.; Nakazawa, Y.; Nishikawa, T.; Kawase, T.; Shimoda, T.; Ogawa, S. Very High-Mobility Organic Single-Crystal Transistors with In-Crystal Conduction Channels. *Appl. Phys. Lett.* **2007**, *90*, 102120.

(55) Sundar, V. C.; Zaumseil, J.; Podzorov, V.; Menard, E.; Willett, R. L.; Someya, T.; Gershenson, M. E.; Rogers, J. A. Elastomeric Transistor Stamps: Reversible Probing of Charge Transport in Organic Crystals. *Science* **2004**, *303*, 1644−1646.

(56) Reese, C.; Bao, Z. High-Resolution Measurement of the Anisotropy of Charge Transport in Single Crystals. *Adv. Mater.* **2007**, *19*, 4535−4538.

(57) Podzorov, V.; Menard, E.; Borissov, A.; Kiryukhin, V.; Rogers, J. A.; Gershenson, M. E. Intrinsic Charge Transport on the Surface of Organic Semiconductors. *Phys. Rev. Lett.* **2004**, *93*, 086602.

(58) Nelson, S. F.; Lin, Y.-Y.; Gundlach, D. J.; Jackson, T. N. Temperature-Independent Transport in High-mobility Pentacene Transistors. *Appl. Phys. Lett.* **1998**, *72*, 1854−1856.

(59) Jurchescu, O. D.; Baas, J.; Palstra, T. T. M. Effect of Impurities on the Mobility of Single Crystal Pentacene. *Appl. Phys. Lett.* **2004**, *84*, 3061−3063.

(60) Meier, T.; Zhao, Y.; Chernyak, V.; Mukamel, S. Polarons, Localization, and Excitonic Coherence in Superradiance of Biological Antenna Complexes. *J. Chem. Phys.* **1997**, *107*, 3876−3893.

(61) Munn, R.; Silbey, R. Theory of Electronic Transport in Molecular Crystals. II. Zeroth Order States Incorporating Nonlocal Linear Electron−Phonon Coupling. *J. Chem. Phys.* **1985**, *83*, 1843−1853.

(62) Munn, R.; Silbey, R. Theory of Electronic Transport in Molecular Crystals. III. Diffusion Coefficient Incorporating Nonlocal Linear Electron−Phonon Coupling. *J. Chem. Phys.* **1985**, *83*, 1854−1864.